EPJ Web of Conferences **126**, 04007 (2016) DOI: 10.1051/epjconf/201612604007
ICNFP 2015

Investigation of particle coherence in Pb+Pb collisions at LHC

Bengt Henrik Brusheim Johansson[1,a]

[1] *Department of Physics, P.b. 1048 Blindern, 0316 Oslo, Norway*

Abstract. The observed particle distributions in Pb+Pb collisions at LHC are investigated. Monte Carlo simulations of the azimuthal anisotropy i.e. flow, and transverse momentum spectra provide insights in e.g. hadron genesis and in medio scattering. Simulations are made using the HYDJET++ model, which is based on parameterization of soft processes and generation of hard physics. The second and third event planes are implemented at this stage, thus generating the second and third order flows which are believed to provide the main part of the observed azimuthal distribution. Here, the ellipticity driven elliptic, and fluctuation driven triangular flow are used as differentiated observables. The elliptic and triangular flow are simulated in agreement with experimental data for $p_T < 3.5$ GeV and centralities $0 - 50\%$. In connection to the simulation of azimuthal anisotropy, the particle transverse momentum spectra are simulated with accuracy, which provides a high degree of reproduction of geometric features. In extension to these simulations, the dependences on fragmentation processes are investigated through the second and third order flows, which are displaying sensitivity to particle coherence. In the simulations, particle coherence is thus seen to manifest itself through the azimuthal anisotropy.

1 Introduction

In processes involving factorization of abstracted observables; *in praegressus* mechanics may be studied by extensive modelling of the evolutionary processes; or of selected parts of it. In the high energy laboratories, the heavy ion collisions are believed to produce exotic phases which consist of partially factorized matter. Experiments at the Relativistic Heavy Ion Collider (RHIC) have rendered evidence of a hot and dense matter produced in the early stages. This phase is hypothesized as a perfect liquid [1–4]; and is the common view of today. The postulated state then undergoes phase transitions when evolving, hadronizing; and later interacting with the particle detectors, thus producing the observed distributions [5, 6]. The (strongly) interacting matter thus displays collectivity in form of e.g. azimuthal anisotropy [7–10]. The fluid postulate suggests a (partially) hydrodynamic description. This description provides a "flow" due to pressure gradients (eccentricity) in the produced fireball (1)

[a] e-mail: bhjohan@uio.no

$$\epsilon_n = -e^{-i\phi_n} \frac{\langle r^n e^{i\phi} \rangle}{\langle r^n \rangle}. \quad (1)$$

Here, the initial state event plane is denoted by ϕ_n and the transverse radius is denoted "r". The eccentricities are believed to evolve from the initial state while undergoing significant *in medio* modulations; thus rendering in an anisotropic momentum distribution; which is described in terms of flow terms (2) in the general momentum distribution (3). Thus; the azimuthal anisotropy provides a main observable in the investigations of *in medio* processes such as jet production and modulation. The mentioned flow-terms corresponds by order n to the terms in (1); and are thus projected as

$$v_n = \langle \cos n(\phi - \Psi_n) \rangle. \quad (2)$$

Here, ϕ and Ψ_n are the observed particle azimuth and the n^{th} event plane angle. The flow terms are projected out of the Fourier expansion [11, 12] of the observed momentum particle distribution as

$$E\frac{d^3N}{d^3p} = \frac{1}{\pi}\frac{d^2N}{dp_T^2 dy}\left[1 + 2\sum_{n=1}^{\infty} v_n \cos n\left(\phi - \Psi_n\right)\right]. \quad (3)$$

Here; the total momenta is p and the transverse momenta and rapidity are denoted by p_T and y. The energy is denoted by E. The flow displays characteristics depending on the order n; i.e. the second order flow depends on the main geometric mode of the initial conditions; i.e. the ellipticity, $n = 2$ in (1). The third order mode; triangularity, is necessarily dependent on fluctuations in the initial energy distribution in order to produce the non-zero flow; due to the odd geometry in (1). Higher order flow, i.e. higher order terms in (3); here represented by the flows of order 4-6, are also expected to display a differentiated behaviour, i.e. sensitivity to fluctuations, thus being of interest. The higher flow-harmonics may be viewed upon as complex objects; thus possibly factorizable. Factorizations of the higher order flow holds information which can be extracted through different projections of the simulations. In this paper; the higher order harmonics [13, 14] are to be examined in the second, third; and fifth order planes [15]; thus providing a base for the simulations of higher order flows. These higher order flows are then related to factorizations of the lower order flows in order to investigate processes through their coherence characteristics. Also; the particle spectra has to be included in the investigations. Thus, the elliptic and the triangular flow are to be implemented in the model in order to simulate a fireball with the main geometric modes; ellipticity and fluctuations in terms of triangularity. The yield is then simulated on the freeze-out hyper surfaces in order to simulate the azimuth and spectra of the heavy ion collisions.

2 Method

In the model used for present paper (HYDJET++); the hydro dynamical processes are parameterized on freeze-out hyper surfaces of the expanding fireball [16, 17]; and forms in superposition with hard particles the simulated distributions. In present model [18, 19], the expanding fireball is modulated by *in medio* collisions [20–22] and radiation [23, 24]. Also, shadowing effects [25] are accounted for in the model. In order to simulate the azimuthal

anisotropy; the fireball transverse radius "R"

$$R\left(b,\phi\right)=R_f\left(b\right)\frac{\sqrt{1-\epsilon^2(b)}}{\sqrt{1+\epsilon(b)\cos 2\phi}}, \tag{4}$$

is modulated in terms of azimuth ϕ and the impact-parameter dependent model-eccentricity $\epsilon(b)$; with R_f as the fireball RMS radius. Also, the linear transverse rapidity profile; and thus the particle velocity are modulated in terms of a second model parameter $\delta\left(b\right)$. The modulation of the transverse velocity u^T is

$$u^x=\sqrt{1+\delta\left(b\right)}\sinh\tilde{\rho_u}\cos\phi,\quad u^y=\sqrt{1-\delta\left(b\right)}\sinh\tilde{\rho_u}\sin\phi, \tag{5}$$

where the transverse rapidity is further modulated by event plane angles, e.g. $\tilde{\rho_u}=\tilde{\rho_u}(\Psi_3)$. In the model, the generation of the third order flow, v_3, is carried out by introducing a model triangularity, ϵ_3. The third event plane is generated uniformly in the model; only weakly correlated with the reaction plane. At this moment; the model does not propagate the initial conditions through an evolution iteration. Thus; the event-by-event fluctuations are quite artificial in the simulations.

3 Results

The momentum azimuthal anisotropy is investigated by projecting the flow terms in (3). These terms are further projected in terms of particle production mode as an attempt to separate different types of coherency. The transverse momentum spectra are simulated for centralities and displayed for reference to abundances and particle production modes. The

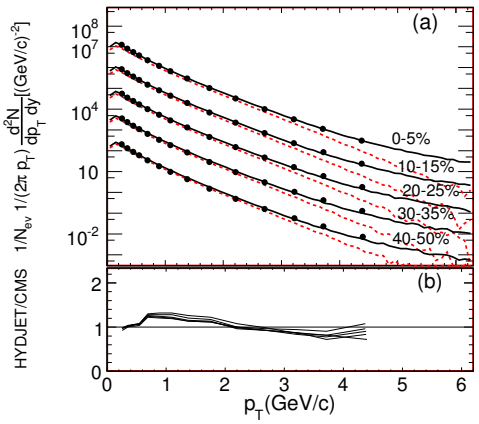

Figure 1. Transverse momentum spectra for unidentified particles (a) (——) and hydro dynamical particles (- - - -). Particle spectra are simulated for: $\sigma/\sigma_{geo}=0-5\%$; $\sigma/\sigma_{geo}=10-15\%$; $\sigma/\sigma_{geo}=20-25\%$; $\sigma/\sigma_{geo}=30-35\%$; and $\sigma/\sigma_{geo}=40-50\%$. Experimental data [6] are denoted by ● . Comparison between experimental data and simulations in the lower pane (b).

particle spectra displays differentiation in transverse momentum in Fig.1a: the lower transverse momentum regime is to a high degree produced in hydrodynamic processes. Due to

this mode, the spectra displays a thermal-exponential nature for the $p_T \leq 2$ GeV/c regime. For the higher transverse momentum regime; the defining particle production mode is fragmentation, which produces a power-law spectrum, differentiated from the thermal part of the spectra. The spectra displays a high degree of accuracy when compared to CMS data [6], as seen in the bottom pane of Fig.1b.

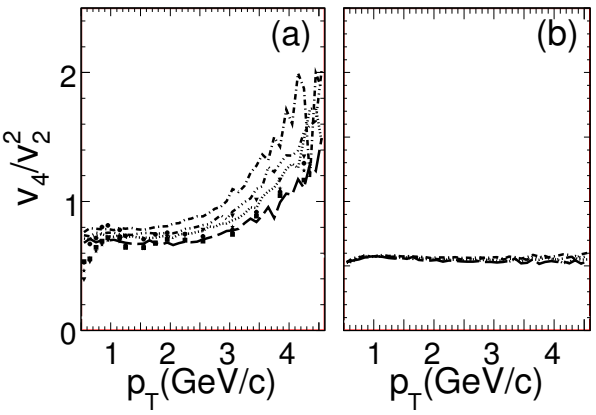

Figure 2. Ratio v_4/v_2^2 for unidentified- (a); and hydro dynamical particles (b). Simulations are made for: $\sigma/\sigma_{geo} = 10-20\%$ (— — —); $\sigma/\sigma_{geo} = 20-30\%$ (· · · · · ·); $\sigma/\sigma_{geo} = 30-40\%$ (— · · —); and $\sigma/\sigma_{geo} = 40-50\%$ (— · —). ALICE [26] data are denoted by: $\sigma/\sigma_{geo} = 10-20\%$ (●); $\sigma/\sigma_{geo} = 20-30\%$ (■); $\sigma/\sigma_{geo} = 30-40\%$ (★); and $\sigma/\sigma_{geo} = 40-50\%$ (▼)

The azimuthal anisotropy is in present paper displayed as higher order flows compared to the corresponding factorization in terms of lower order flows. The v_4 flow is simulated in the model Ψ_2 plane; and is compared to the factorization $v_2 v_2$. The ratio is also compared to experimental ALICE data [26] (Fig.2a); due to the available ALICE $v_4(\Psi_2)$ projection. The agreement with experimental data is fair; although deviations are seen for centralities. The experimental data seem to scale for centralities to a greater extent than the simulations with an ATLAS setting might indicate. This feature is likely due to the absence of a model Ψ_4 plane. The Ψ_4 plane might then provide a higher degree of scaling for the simulated ratio (Fig.2b); due to higer correlation to jets. The fourth order Ψ_2 flow displays scaling; largely depending on the common event plane. The ratio is seen to be weakly dependent on centrality due to elevated fluctuation levels. It is also seen in the simulations that the ratio acts as an observer of jet-production (Fig.2) [27]. Further; a fifth order model event plane is established in order to investigate the pentagonal (v_5) flow compared to its $v_2 v_3$ factorization, and also the effect of the event plane mixing. The inclusive $v_5/v_3 v_2$ ratio displays in Fig.3a; a fair level of agreement with experimental data [5]. The greatest prediction power of the model seems to be located at the mid- and low ($p_T \leq 3$ GeV/c) regime. The experimental ratio displays high levels of fluctuations; thus difficult to analyse at this stage. Some deviations are also seen for centralities; in particular for the central $10-20\%$ hits. The hydro dynamical projection in Fig.3b of the ratio displays a weak or non-existent scaling for transverse momentum and centralities due to coherency from the elliptic plane as seen from the ratio hierarchy. The

planes are thus seen to correlate weakly. Jets are seen to elevate the ratio; even for the lower transverse momentum regime due to the fluctuation dependence of the ratio.

In connection to the simulation of the v_5/v_3v_2 plane; the effects of event plane mixing is studied through the $v_5(\Psi_2, \Psi_3)/v_3v_2$ ratio. For the fifth order, mixed event plane; flow is also simulated using combinations of the second and third event plane as of Fig.4a. The simulations display a reverse centrality hierarchy compared to the "plain" fifth order ratio. The elliptic plane provides coherency which counteracts the fluctuation dependent behaviour of the ratio. Here; the hydrodynamic projection, displayed in Fig.4b displays scaling both in transverse momentum and centrality in contrast to the case of non-event plane mixing. This is due to wave number coherence scaling: similar to the case of Fig.2b. It is now seen that the jets provides the ratio hierarchy. In order to move the investigation of correlators forward; the sixth order factorization v_3^2/v_2^3 is investigated for inclusive particles and also as a hydro dynamical projection. The flow displays weak scaling and dependence of transverse momentum and a strong centrality dependence due to the fluctuation/coherence nature of the ratio; similar to the case of Fig.5. The agreement with experimental data is high (Fig.5a). In particular for the more peripheral "tuned" hits. The hydro dynamical projection; displayed in Fig.5b displays a strong ellipticity dependence due to the differentiation in coherency. Jet production is thus seen to provide for an approximate transverse momentum wave-number scaling.

4 Discussion and Conclusion

The simulations of the higher order flows display a high degree of reproduction. The second, third; and fifth order flows are fully implemented in the model thus exhibiting a high degree

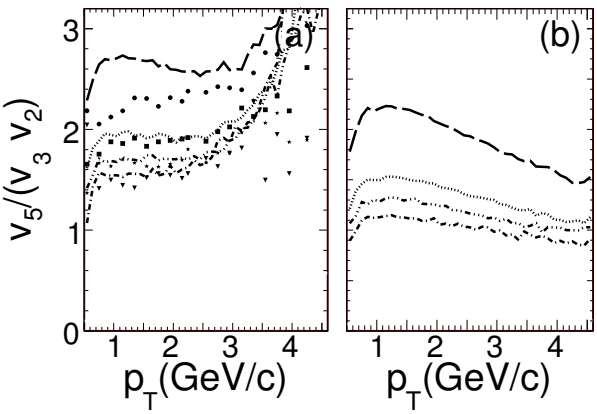

Figure 3. Ratio $\frac{v_5}{v_2v_3}$ for unidentified- (a); and hydro dynamical particles (b). Simulations are made for: $\sigma/\sigma_{geo} = 10-20\%$ (— — —); $\sigma/\sigma_{geo} = 20-30\%$ (· · · · · ·); $\sigma/\sigma_{geo} = 30-40\%$ (— · · —); and $\sigma/\sigma_{geo} = 40-50\%$ (— · —). Experimental data are included for comparison [5]. The data are denoted by: $\sigma/\sigma_{geo} = 10-20\%$ (●); $\sigma/\sigma_{geo} = 20-30\%$ (■); $\sigma/\sigma_{geo} = 30-40\%$ (★); and $\sigma/\sigma_{geo} = 40-50\%$ (▼)

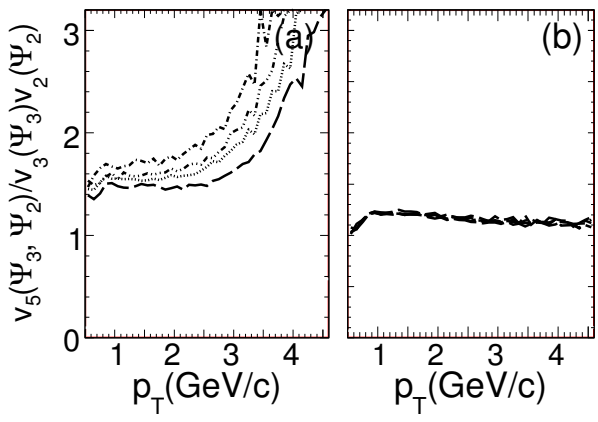

Figure 4. Ratio $\frac{v_5(\Psi_2,\Psi_3)}{v_2 v_3}$ for unidentified- (a); and hydro dynamical particles (b). Simulations are made for: $\sigma/\sigma_{geo} = 10-20\%$ (— — —); $\sigma/\sigma_{geo} = 20-30\%$ (· · · · · ·); $\sigma/\sigma_{geo} = 30-40\%$ (— · · —); and $\sigma/\sigma_{geo} = 40-50\%$ (— · —). Data are denoted by: $\sigma/\sigma_{geo} = 10-20\%$ (●); $\sigma/\sigma_{geo} = 20-30\%$ (■); $\sigma/\sigma_{geo} = 30-40\%$ (★); and $\sigma/\sigma_{geo} = 40-50\%$ (▼)

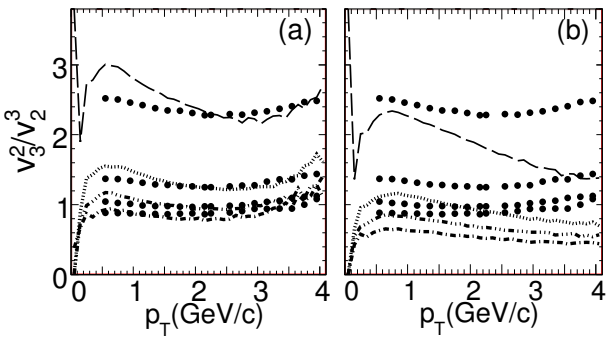

Figure 5. Ratio v_3^2/v_2^3 for unidentified- (a); and hydro dynamical particles (b). Experimental data for inclusive particles are included for comparison [5] and are denoted by ● . Simulations are made for: $\sigma/\sigma_{geo} = 10-20\%$ (— — —); $\sigma/\sigma_{geo} = 20-30\%$ (· · · · · ·); $\sigma/\sigma_{geo} = 30-40\%$ (— · · —); and $\sigma/\sigma_{geo} = 40-50\%$ (— · —).

of accuracy. The simulations of these particular flows are thus believed to represent a high degree of robustness and reliability. The flow ratios are displaying two fundamental types of behaviour. First; the mixed event plane type; which displays hydro dynamical factorization. The hydro dynamical flow is here seen as factorized due to the common event plane and the absence of jet fluctuations, thus nullifying the differentiation in coherency. This common

factorization seems to represent the geometric limit. Fluctuations are thus seen to form the mixed event plane centrality hierarchy alone in the model.

Second; the non-mixed event plane ratios displays a dependence on transverse momentum and also centrality due to the skewness in wavenumbers and geometric mode (coherence). The centrality hierarchy is here seen as strongly coherence dependent in contrast to the case of event plane mixing. *In conclusion*; the pure and event plane mixed flow displays differences in the level of factorization in the model. Thus, fluctuations are the only provider of flow hierarchy for the mixed event plane flow. Pure flow depends on initial geometry; thus displaying the relations between the event planes.

Acknowledgements

The author wish to thank his supervisors L. Bravina, E. E. Zabrodin; and the associated research group. The author also wish to thank the ICNFP2015 organizing committee; and the people of Crete for an amazing conference and an awe-inspiring visit.

References

[1] I. Arsene et al., Nucl. Phys. A **757**, 1 (2005)
[2] B.B. Back et al., Nucl. Phys. A **757**, 28 (2005)
[3] J. Adams et al., Nucl. Phys. A **757**, 102 (2005)
[4] K. Adcox et al., Nucl. Phys. A **757**, 184 (2005)
[5] G. Aad et al., Phys. Rev. C **86**, 014907 (2012)
[6] S. Chatrchyan et al., Phys. Rev. C **87**, 014902 (2013)
[7] U. Heinz, R. Snellings, Annu. Rev. Nucl. Part. Sci. **63**, 123 (2013)
[8] S.A. Voloshin, Nucl. Phys. A **904-905**, 90c (2013)
[9] H.G. Ritter, R. Stock, J. Phys. G: Nucl. Part. Phys. **41**, 124002 (2014)
[10] R. Snellings, J. Phys. G: Nucl. Part. Phys. **41**, 124007 (2014)
[11] S. Voloshin, Y. Zhang, Z. Phys. C **70**, 665 (1996)
[12] A.M. Poskanzer, S.A. Voloshin, Phys. Rev. C **58**, 1671 (1998)
[13] J. Velkovska, J. Phys. G: Nucl. Part. Phys. **38**, 124011 (2011)
[14] J. Jia, J. Phys. G: Nucl. Part. Phys. **38**, 124012 (2011)
[15] L. Bravina, B.H. Brusheim Johansson, E.E. Zabrodin, G. Eyyubova, V.L. Korotkikh, I.P. Lokhtin, L.V. Malinina, S.V. Petrushanko, A.M. Snigirev, Phys. Rev. C **89**, 024909 (2014)
[16] N.S. Amelin, R. Lednicky, I.P. Lokhtin, L.V. Malinina, A.M. Snigirev, I.A. Karpenko, Y.M. Sinyukov, I. Arsene, L. Bravina, Phys. Rev. C **74**, 064901 (2006)
[17] N.S. Amelin, R. Lednicky, T.A. Pocheptsov, I.P. Lokhtin, L.V. Malinina, A.M. Snigirev, I.A. Karpenko, Y.M. Sinyukov, Phys. Rev. C **77**, 014903 (2008)
[18] I.P. Lokhtin, A.M. Snigirev, Eur. Phys. J. C **45**, 211 (2006)
[19] I.P. Lokhtin, L.V. Malinina, S.V. Petrushanko, A.M. Snigirev, I. Arsene, K. Tywoniuk, Comp. Phys. Comm. **180**, 779 (2009)
[20] J.D. Bjorken, FERMILAB-PUB-82/59-THY (1982)
[21] E. Braaten, M. Thoma, Phys. Rev. D **44**, 1298 (1991)
[22] I.P. Lokhtin, A.M. Snigirev, Eur. Phys. J. C **16**, 527 (2000)

[23] R. Baier, Y.L. Dokshitzer, A.H. Mueller, D. Shiff, Phys. Rev. C **60**, 064902 (1999)
[24] R. Baier, Y.L. Dokshitzer, A.H. Mueller, D. Shiff, Phys. Rev. C **64**, 057902 (2001)
[25] K. Tywoniuk, I. Arsene, L. Bravina, A.B. Kaidalov, E. Zabrodin, Phys. Lett. B **657**, 170 (2007)
[26] B. Abelev et al., Phys. Lett. B **719**, 18 (2013)
[27] L. Bravina, B.H. Brusheim Johansson, G. Eyyubova, E.E. Zabrodin, Phys. Rev. C **87**, 034901 (2013)